II CONGRESSO NACIONAL DE ENGENHARIA MECÂNICA
II NATIONAL CONGRESS OF MECHANICAL ENGINEERING
12 a 16 de Agosto de 2002 - João Pessoa – PB

TURBULENT FLOW IN A CORRUGATED CHANNEL USING LINEAR AND NON-LINEAR k-ε MODELS WITH HIGH AND LOW REYNOLDS FORMULATIONS

Marcelo Assato – e-mail: assato@mec.ita.br
Marcelo J.S. De-Lemos – e-mail: delemos@mec.ita.br
Departamento de Energia - IEME, Instituto Tecnológico de Aeronáutica - ITA
12228-900 São José dos Campos - SP - Brazil

Abstract. *This work examines the performance of linear and non-linear eddy-viscosity models when used to predict turbulent flow in a periodically sinusoidal-wave channel. The geometry of a channel with converging-diverging walls is investigated for a Reynolds number of 40000. The numerical method employed for the discretization of the equations is the control-volume method applied in a boundary-fitted non-orthogonal coordinate system. The SIMPLE algorithm is used for correction of the pressure field. The classical wall function or a low Reynolds model is used to describe the flow near the wall. Comparisons among those two approaches using the linear and non-linear turbulence models are done. Here, an implicit numerical treatment is proposed for handling the non-linear diffusion terms of the momentum equations. Such a procedure aims at the increase of the robustness of the solution method.*

Keywords: *Turbulence modeling; Non-linear models; sinusoidal-wave channels; Control-volume method; Implicit treatment.*

1. INTRODUCTION

The analysis of flow over wave boundaries is of great interest in the engineering field. Several phenomena involving wave boundaries occur in the nature, as: generation of wind waves on water; evolution of sand dunes in deserts and sediment dunes in rivers, etc (Patel et al., 1991). Some industrial devices make use of sinusoidal walls. Development of high-performance thermal system has received much attention in the last years. Modified surfaces are required to reduce the size and weight of heat exchanging devices such as those encountered in electronic cooling, air-conditioning, automobiles, aircrafts and spacecrafts, etc. In accordance with Habib et al. (1998) there are many different ways of increasing heat and mass transfer, using generating surfaces of turbulence (zigzag-type, cavity-type, grooved-type, staggered ribs-type, etc). Various researchers studied experimentally the turbulent flow over wave boundaries. Hsu and Kennedy (1971) investigated the axisymmetric flow in a circular pipe, where the diameter varies sinusoidally along its length. Zilker et al. (1977), Buckels et al. (1984) measured the shear stress and velocity profile in a channel with sinusoidally varying, wavy wall bottom. Saniei and Dini (1993) measured the pressure drop, velocity profile and local heat transfer. They presented the friction factor and local Nusselt number for the periodically converging-diverging rectangular channel using three different aspect ratios, and Reynolds number ranging from 10^4 to 10^5. Hanratty et al. (1983) studied numerically the turbulent flow in a channel with sinusoidal bottom surface and Patel et al. (1991) investigated a rectangular channel using different amplitudes. Habib et al. (1998) simulated the geometry of sinusoidally converging-diverging channel. They used the two-equation (linear $k-\varepsilon$) eddy-

viscosity model and presented the velocity and streamline distributions, the kinetic energy of turbulence, pressure drop, friction factor, and local, average and maximum Nusselt number distribution for Reynolds numbers from $4x10^4$ to 10^5.

It is well established in the literature that linear eddy-viscosity turbulence models (LEVM) do not, on the whole, cope well with strong streamline curvature whether it arises from flow over curved surfaces or imparted swirling. And yet, turbulence-driven secondary motion and directional effects due to buoyancy cannot, due to absence of information on individual stresses, be fully simulated with LEVMs. In spite of that, they are often used for engineering computations due to the numerical robustness obtained via its linear *stress-strain rate* relationship (Jones and Launder, 1972). This diffusion-like approach makes the numerical solution stable, with the model easily adaptable to existing computer code architectures.

Models involving other types of constitutive equations have been lately developed with the perspective of applying CFD to complex flows. These techniques aim at a wider range of applicability, similar to that of Reynolds Stress Models (RSM, Launder et al., 1975) while keeping computational costs down to LEVM cost levels. Theories employing other type of representation of individual Reynolds Stresses/Fluxes, including addition of non-linear terms to the basic constitutive equation, try to capture the sensitivity to flow curvatures and buoyancy, a feature missing in basic LEVMs.

To the best of the authors' knowledge, most published work on non-linear models (Speziale, 1987, Nisizima and Yoshizawa, 1987, Rubinstein and Barton, 1990, Shih et al., 1993, Gatski and Speziale, 1993) are either written for Cartesian coordinates and/or treat additional non-linear terms in a fully explicit manner. The literature has commented on the difficulties of convergence of the solution when non linear turbulence models are used in complex flows, such as the numerical works by Abid et al. (1995), Rahman et al. (1997) and Bauer et al. (2000). Here, a *new* numerical treatment is proposed to handle a general non-linear constitutive equation into a boundary-fitted computer code. The numerical methodology proposed herein contributes to the robustness of the solution method and increases the applicability of such non-linear models to numerical grids fully complacent with irregular computational domains. The treatment consists in splitting the non linear diffusive fluxes in an implicit term in the coefficients matrix and explicit gathering in the source term. In the literature, there aren't specific information on the numerical treatment of these non linear terms.

This work has two objectives: (i) to analyse the performance of linear and non-linear eddy-viscosity models in a generalized coordinate system in the prediction of turbulent flow in periodically sinusoidal-wave channels using the classical wall function and low Reynolds damping functions for handling wall proximity. (ii) to investigate the computational robustness of implicit numerical treatment proposed by authors.

2. TWO-EQUATION MODEL FOR VELOCITY FIELD

The governing equations to be solved are the continuity and the Reynolds-averaged Navier-Stokes equations which take the form

$$\frac{\partial U_i}{\partial x_i} = 0 \ , \tag{1}$$

$$\rho U_j \frac{\partial U_i}{\partial x_j} = \frac{\partial \tau_{ij}}{\partial x_j} - \frac{\partial P}{\partial x_i}, \tag{2}$$

where U_i is the mean velocity component in the *i*-direction, ρ is the density of the fluid. For easy of computation, the total pressure $P = p + \frac{2}{3}\rho k$ involves also a term containing the turbulent kinetic energy $k = \overline{u_i' u_i'}/2$ where u_i' is the fluctuating part of the instantaneous velocity in the *i*-direction.

The stress τ_{ij} represents the sum of the turbulent stress, τ_{ij}^{t}, plus the laminar viscous stress, $\tau_{ij}^{\ell} = \mu S_{ij}$, where the deformation tensor is given by,

$$S_{ij} = \left(\frac{\partial U_i}{\partial x_j} + \frac{\partial U_j}{\partial x_i} \right). \tag{3}$$

Different constitutive equations for the Reynolds stress will be discussed later and they shall be classified basically as Linear and Non-Linear relationships.

The modeled transport equations for the turbulent kinetic energy *k*, and its dissipation rate ε, respectively, are given by:

$$U_i \frac{\partial k}{\partial x_i} = \frac{\partial}{\partial x_i}\left(\frac{\mu_t}{\rho \sigma_k} \frac{\partial k}{\partial x_i} \right) + P_k - \varepsilon , \tag{4}$$

$$U_i \frac{\partial \varepsilon}{\partial x_i} = \frac{\partial}{\partial x_i}\left(\frac{\mu_t}{\rho \sigma_\varepsilon} \frac{\partial \varepsilon}{\partial x_i} \right) + c_1 \frac{\varepsilon}{k} P_k - c_2 f_2 \frac{\varepsilon^2}{k} . \tag{5}$$

The symbols P_k and μ_t, respectively, represent the turbulence kinetic energy production rate and the eddy viscosity, and are defined as:

$$P_k = \tau_{ij}^{t} \frac{\partial U_i}{\partial x_j}, \qquad \mu_t = c_\mu f_\mu \rho \frac{k^2}{\varepsilon}. \tag{6}$$

In the present work, both high and low Reynolds models are compared. Their basic difference lies in the distinct form of the damping functions f_2 and f_μ referred in Eqs. (5) and (6). Expressions for them are shown in Tab. (1). These functions and a slightly different set of constants were used in conjunction with the *k*-ε equations.

In calculating the wall shear stress with the high Reynolds method (Launder and Spalding, 1974), *E* in Tab. (1) may be varied to simulate the surface roughness and $\kappa = 0.41$ is the von Kármán constant. Subscript *P* refers to the node next to the wall. Thus u_P and k_P are, respectively, the value of the velocity and turbulent kinetic energy in this point, and y_P is the normal distance to the wall. The symbol *n* in the low Reynolds model represents the normal distance to the wall. The

Table 1. High and Low Reynolds Models

	High Reynolds model proposed by Launder and Spalding (1974)	Low Reynolds model proposed by Abe *et al* (1992)
f_μ	1.0	$\left\{1-\exp\left[-\frac{(\nu\varepsilon)^{0.25} n}{14\nu}\right]\right\}^2 \left\{1+\frac{5}{(k^2/\nu\varepsilon)^{0.75}}\exp\left[-\left(\frac{(k^2/\nu\varepsilon)}{200}\right)^2\right]\right\}$
f_2	1.0	$\left\{1-\exp\left[-\frac{(\nu\varepsilon)^{0.25} n}{3.1\nu}\right]\right\}^2 \left\{1-0.3\exp\left[-\left(\frac{(k^2/\nu\varepsilon)}{6.5}\right)^2\right]\right\}$
τ_w	$\frac{u_P \rho c_\mu^{\frac{1}{4}} \kappa k_P^{\frac{1}{2}}}{\ln\left(\frac{E\rho c_\mu^{\frac{1}{4}} k_P^{\frac{1}{2}} y_P}{\mu}\right)}$	$\mu \frac{\partial u}{\partial y}$

constants c_μ, c_1, c_2, σ_k and σ_ε for the high Reynolds model are set as 0.09, 1.44, 1.92, 1.0 and 1.33, respectively, and for the low Reynolds model given by 0.09, 1.5, 1.9, 1.4 and 1.3, respectively.

In this work, the linear and non-linear eddy-viscosity models are analyzed. For the linear $k-\varepsilon$ model of turbulence, the Reynolds stress tensor is assumed to be of the form

$$\tau_{ij}^t = \mu_t S_{ij} - \tfrac{2}{3}\rho\delta_{ij}k\,. \tag{7}$$

As mentioned before, the last term in (7) was compacted into an expression for the total pressure.

Non-linear eddy-viscosity models originated in a general proposal done by Pope (1975). However, only in the past two decades such models have had great progresses with the works of Speziale (1987), Nisizima and Yoshizawa (1987), Rubinstein and Barton (1990), Shih et al (1993), among others. In these works, quadratic products were introduced involving the strain and vorticity tensors with different derivations and calibrations for the models. These quadratic forms produce a certain anisotropy degree among the normal tensions, which make possible to predict, among other processes, the presence of secondary motion in non-circular ducts.

A general non-linear expression for the Reynolds stress, kept to second order, can be written as:

$$\begin{aligned}\tau_{ij}^t = &\left(\mu_t\, S_{ij}\right)^L - \left(c_{1NL}\,\mu_t\,\frac{k}{\varepsilon}\left[S_{im}S_{mj} - \tfrac{1}{3}S_{ml}S_{ml}\delta_{ij}\right]\right)^{NL1} \\ &-\left(c_{2NL}\,\mu_t\,\frac{k}{\varepsilon}\left[\Omega_{im}S_{mj} + \Omega_{jm}S_{mi}\right]\right)^{NL2} - \left(c_{3NL}\,\mu_t\,\frac{k}{\varepsilon}\left[\Omega_{im}\Omega_{jm} - \tfrac{1}{3}\Omega_{lm}\Omega_{lm}\delta_{ij}\right]\right)^{NL3}\end{aligned} \tag{8}$$

where the *c*'s are constants or coefficients, δ_{ij} is the Kronecker delta; the superscripts in Eq. (8) indicate **L**inear and **N**on **L**inear contributions, S_{ij} is the deformation tensor given by (3) and Ω_{ij} represents the vorticity tensor written as

$$\Omega_{ij} = \left(\frac{\partial U_i}{\partial x_j} - \frac{\partial U_j}{\partial x_i}\right). \tag{9}$$

Equation (8) already assumes that the term $\frac{2}{3}\rho\delta_{ij}k$ is combined into the total pressure *P*. In this work the non-linear model proposed by Shih et al (1993) was used and has the following expressions:

$$c_\mu = \frac{2/3}{1.25 + s + 0.9\Omega}, \qquad c_{1NL} = \frac{0.75}{c_\mu\left(1000 + s^3\right)}, \quad c_{2NL} = \frac{3.8}{c_\mu\left(1000 + s^3\right)}, \quad c_{3NL} = \frac{4.8}{c_\mu\left(1000 + s^3\right)},$$

where,

$$s = \frac{k}{\varepsilon}\sqrt{\tfrac{1}{2}S_{ij}S_{ij}} \qquad \text{and} \qquad \Omega = \frac{k}{\varepsilon}\sqrt{\tfrac{1}{2}\Omega_{ij}\Omega_{ij}} \tag{10}$$

3. NUMERICAL METHOD AND IMPLICIT TREATMENT

The numerical method employed for discretizing the governing equations is the control-volume approach in a generalized coordinate system with a collocated grid. For a solution of pressure linked through continuity equation, SIMPLE algorithm is used. A hybrid scheme, Upwind Differencing

Scheme (UDS) and Central Differencing Scheme (CDS), is used for interpolating the convection fluxes.

Figure 1 shows a typical control-volume with detailed notation, distances and indexing used when transforming the original equations into the $\eta - \xi$ coordinate system. With the help of this figure, the following operators can be identified:

$$\Delta x_{\eta}^{e} = (x_{ne} - x_{se}), \quad \Delta x_{\xi}^{e} = (x_{E} - x_{P}), \quad \Delta y_{\eta}^{e} = (y_{ne} - y_{se}), \quad \Delta y_{\xi}^{e} = (y_{E} - y_{P}), \tag{11}$$

$$\Delta x_{\xi}^{n} = (x_{ne} - x_{nw}), \quad \Delta x_{\eta}^{n} = (x_{N} - x_{P}), \quad \Delta y_{\xi}^{n} = (y_{ne} - y_{nw}), \quad \Delta y_{\eta}^{n} = (y_{N} - x_{P}). \tag{12}$$

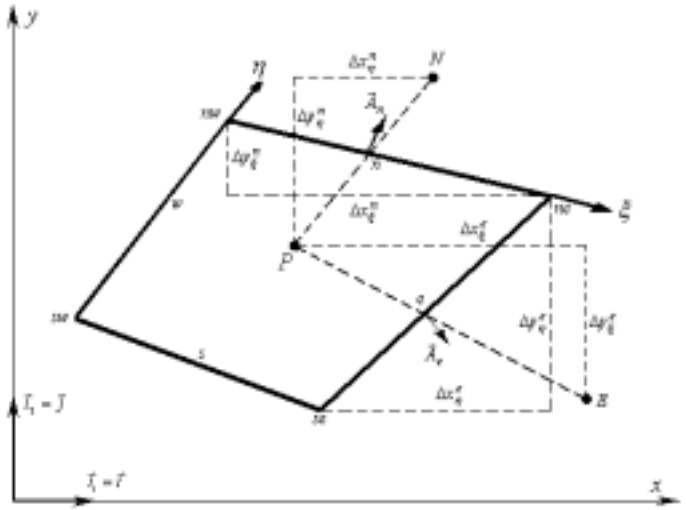

Figure 1- Control-volume and notation

The vector form of the area of the control-volume at *east* and *north* faces, respectively, are given by

$$\vec{A}_e = \Delta y_{\eta}^{e}\vec{i} - \Delta x_{\eta}^{e}\vec{j}, \qquad \vec{A}_n = -\Delta y_{\xi}^{n}\vec{i} + \Delta x_{\xi}^{n}\vec{j}. \tag{13}$$

Semi-implicit treatment of the diffusive terms. The whole numerical treatment and discretization process of convection/diffusion linear/non-linear terms of the momentum equation, as well as the equations for k and ε, are shown in detail in the work by Assato and de Lemos (1998). The numerical treatment presented there for non-linear diffusive terms was totally explicit, accommodating all terms into the source term. In the work by Assato and de Lemos (2001), these same terms were rewritten identifying implicit and explicit parts with the purpose of improving the numerical stability. Thus, the non-linear diffusive terms are rewritten in the following way:

$$\left(I_e^{D_x}\right)^{L} = \Delta U_{\xi}^{e}\left(D_e^{x,y}\right)^{L} + \left(S_e^{*_x}\right)^{L}, \qquad \left(I_e^{D_x}\right)^{NL1} = -\Delta U_{\xi}^{e}\left(D_e^{x,y}\right)^{NL1} - \left(S_e^{*_x}\right)^{NL1}, \tag{14}$$

$$\left(I_e^{D_x}\right)^{NL2} = -\Delta U_{\xi}^{e}\left(D_e^{x,y}\right)^{NL2} - \left(S_e^{*_x}\right)^{NL2}, \qquad \left(I_e^{D_x}\right)^{NL3} = -\Delta U_{\xi}^{e}\left(D_e^{x,y}\right)^{NL3} - \left(S_e^{*_x}\right)^{NL3}. \tag{15}$$

The first terms on the right hand side of Eqs. (14)-(15) are here treated implicitly (in coefficients matrix) whereas the other ones are handled explicitly (in the source term). The coefficients $\left(D_e^{x,y}\right)$ are the same for the equations in x and y and are given by:

$$\left(D_e^{x,y}\right)^{L} = \frac{(\mu + \mu_t)}{\Pi_e}\left[\left(\Delta y_{\eta}^{e}\right)^2 + \left(\Delta x_{\eta}^{e}\right)^2\right], \tag{16}$$

$$\left(D_e^{x,y}\right)^{NL1} = \frac{c_{1NL}\mu_t^e k}{\left(\Pi_e\right)^2 \varepsilon}\left\{-2\left(\Delta y_\eta^e\right)^2 \pi_a^e + 2\Delta x_\eta^e\left[\tfrac{4}{3}\Delta y_\eta^e\left(\pi_b^e + \pi_c^e\right) - \Delta x_\eta^e \pi_d^e\right]\right\}, \tag{17}$$

$$\left(D_e^{x,y}\right)^{NL2} = \frac{2c_{2NL}\mu_t^e k}{\left(\Pi_e\right)^2 \varepsilon}\left\{\Delta x_\eta^e \Delta y_\eta^e\left[\Delta x_\xi^e \Delta U_\eta^e - \Delta y_\xi^e \Delta V_\eta^e\right]\right\}, \tag{18}$$

$$\left(D_e^{x,y}\right)^{NL3} = \frac{c_{3NL}\mu_t^e k}{\left(\Pi_e\right)^2 \varepsilon}\left\{\Delta x_\eta^e \Delta y_\eta^e\left(\pi_b^e + \pi_c^e\right)\right\}. \tag{19}$$

The parts treated explicitly $\left(S_e^{*_x}\right)$ make use of velocity values at grid points calculated at the previous iteration. For the east face and *x*-direction one has:

$$\left(S_e^{*_x}\right)^L = \frac{\left(\mu + \mu_t^e\right)}{\Pi_e}\left\{\left(\Delta U_\xi^e\right)^\circ \left(\Delta y_\eta^e\right)^2 - \left(\Delta U_\eta^e\right)^\circ \left[2\Delta y_\xi^e \Delta y_\eta^e + \Delta x_\xi^e \Delta x_\eta^e\right] - \pi_c^e \Delta x_\eta^e\right\}, \tag{20}$$

$$\left(S_e^{*_x}\right)^{NL1} = -\frac{c_{1NL}\mu_t^e k}{\left(\Pi_e\right)^2 \varepsilon}\left\{\begin{array}{l} -2\Delta y_\eta^e\left[\begin{array}{l} \tfrac{1}{3}\left(\pi_a^e\right)^2 + \left(\Delta U_\eta^e\right)^\circ\left(\begin{array}{l} -\Delta y_\xi^e \pi_a^e + \\ \Delta x_\xi^e\left(\tfrac{1}{3}\pi_c^e + \tfrac{1}{6}\Delta x_\xi^e\left(\Delta U_\eta^e\right)^\circ\right)\end{array}\right) - \tfrac{2}{3}\left(\pi_d^e\right)^2 \\ + \tfrac{1}{6}\left(\pi_c^e\right)^2 \end{array}\right] \\ + 2\Delta x_\eta^e\left[\begin{array}{l} \tfrac{1}{6}\Delta x_\eta^e\left(\Delta U_\xi^e\right)^\circ \pi_a^e + \left(\Delta U_\eta^e\right)^\circ\left(\begin{array}{l} \Delta x_\xi^e \pi_d^e - \\ \Delta y_\xi^e\left(\pi_c^e + \tfrac{7}{6}\pi_b^e - \tfrac{1}{6}\Delta x_\xi^e\left(\Delta U_\eta^e\right)^\circ\right)\end{array}\right) \\ + \pi_c^e \pi_d^e \end{array}\right] \end{array}\right\} \tag{21}$$

$$\left(S_e^{*_x}\right)^{NL2} = -\frac{2c_{2NL}\mu_t^e k}{\left(\Pi_e\right)^2 \varepsilon}\left\{-\Delta y_\eta^e\left[\left(\Delta x_\xi^e\right)^2\left(\left(\Delta U_\eta^e\right)^\circ\right)^2 - \left(\pi_c^e\right)^2\right] + \Delta x_\eta^e\left[\begin{array}{l} \left(\Delta y_\eta^e\right)^2\left(\Delta U_\xi^e\right)^\circ\left(\Delta V_\xi^e\right)^\circ + \\ \left(\pi_b^e - \pi_c^e\right)\left(\Delta y_\xi^e\left(\Delta U_\eta^e\right)^\circ\right) + \pi_d^e \end{array}\right]\right\}, \tag{22}$$

$$\left(S_e^{*_x}\right)^{NL3} = -\frac{c_{3NL}\mu_t^e k}{\left(\Pi_e\right)^2 \varepsilon}\left\{-\frac{\Delta y_\eta^e}{3}\left[\begin{array}{l} \Delta x_\eta^e\left(\pi_b^e + 3\pi_c^e - \Delta x_\eta^e\left(\Delta U_\xi^e\right)^\circ\right)\left(\Delta U_\xi^e\right)^\circ \\ -2\pi_b^e \pi_c^e + \left(\pi_c^e\right)^2 + \left(\Delta x_\xi^e\right)^2\left(\Delta U_\eta^e\right)^\circ \end{array}\right]\right\}. \tag{23}$$

The superscript "°" of velocity differences indicates that these values are taken from the previous iteration. Coefficients π's and Π's are also calculated with velocities from previous iteration.

$$\begin{array}{ll} \Pi_e = \Delta y_\eta^e \Delta x_\xi^e - \Delta y_\xi^e \Delta x_\eta^e; & \\ \pi_a^e = \Delta y_\eta^e\left(U_E - U_P\right) - \Delta y_\xi^e\left(U_{ne} - U_{se}\right); & \pi_b^e = \Delta x_\xi^e\left(U_{ne} - U_{se}\right) - \Delta x_\eta^e\left(U_E - U_P\right); \\ \pi_c^e = \Delta y_\eta^e\left(V_E - V_P\right) - \Delta y_\xi^e\left(V_{ne} - V_{se}\right); & \pi_d^e = \Delta x_\xi^e\left(V_{ne} - V_{se}\right) - \Delta x_\eta^e\left(V_E - V_P\right); \end{array} \tag{24}$$

It is important to notice that for orthogonal grids some geometric distances given by Eqs. (11) and (12) are null, for instance, $\Delta x_\eta^e = \Delta y_\xi^e = \Delta x_\xi^n = \Delta y_\eta^n = 0$. Thus, the equations (16)-(19) for east face become,

$$\left(D_e^{x,y}\right)^L \approx \frac{\left(\mu + \mu_t^e\right)}{\Pi_e}\left[\left(\Delta y_\eta^e\right)^2\right], \qquad \left(D_e^{x,y}\right)^{NL1} \approx c_{1NL}\frac{\mu_t^e k}{\left(\Pi_e\right)^2 \varepsilon}\left\{-2\left(\Delta y_\eta^e\right)^2 \frac{\Delta U_\xi^e}{\Delta x_\xi^e}\right\}, \tag{25}$$

$$\left(D_e^{x,y}\right)^{NL2} \approx 0, \qquad \left(D_e^{x,y}\right)^{NL3} \approx 0. \tag{26}$$

Only the linear and first non-linear terms are added in coefficient matrix.

4. RESULTS

The geometry analyzed is shown in Fig. 2. The geometrical parameters are the channel height, $H_{max} = 10.16\,cm$, the wavelength, $\lambda = 6.667\,cm$ and aspect ratio $2a/\lambda = 0.27$, where a represents the wave-amplitude.

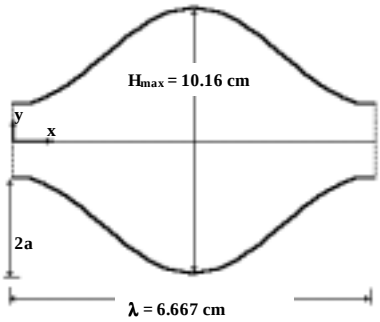

Figure 2 – Geometry of periodically symmetric converging-diverging channel.

The results presented in this section were obtained using a total of four different models. The following turbulence closures were applied: the *linear* and *non-linear* k-ε models using the high Reynolds approach, designated here by **L_HRN** and **NL_HRN**, respectively, and the same models applying the low Reynolds model, named respectively by **L_LRN** and **NL_LRN**. The periodic boundary condition was applied until the fully developed regime was simulated The non-linear model employed was the Shih et al (1993) closure. Figure 3 shows the computational grids used for the High and Low Reynolds formulations.

(a) (b)

Figure 3: Computational grids of symmetric converging-diverging channel for $2a/\lambda = 0.27$.

(a) High Reynolds model (50x22), (b) Low Reynolds model (50x46).

Comparisons for the pressure drop in converging-diverging channel among the present models with experimental data by Saniei and Dini (1993) are shown in Table 2. It can be noticed that smaller deviations are presented by the low Reynolds number formulation with the best prediction obtained by the NL_LRN model. In this work, calculations were performed only for Reynolds number based on hydraulic diameter of Re=40000.

Figure 4 shows the mean velocity field U/U_{avg} in several stations along the channel. All models present small differences, except in first and last station. Included in Fig. (4) are the distributions obtained numerically by Habib et al. (1998).

Figures 5 and 6 show, respectively, dimensionless axial velocity and turbulent kinetic energy distributions using the four turbulence models. It can be noticed that bigger deviations among the results occur when changing the wall treatment from high to the low Reynolds number approach.

Table 2: Pressure drop in periodically symmetric converging-diverging channel.

Results	Pressure drop: $\Delta P \left[N/m^2\right]$	Deviations [%]: $\Delta P \left[N/m^2\right]$
Saniei and Dini (1993)	12.5	-
L_HRN	9.824	21.4
NL_HRN	10.016	19.87
L_LRN	11.243	10.06
NL_LRN	13.553	-8.42

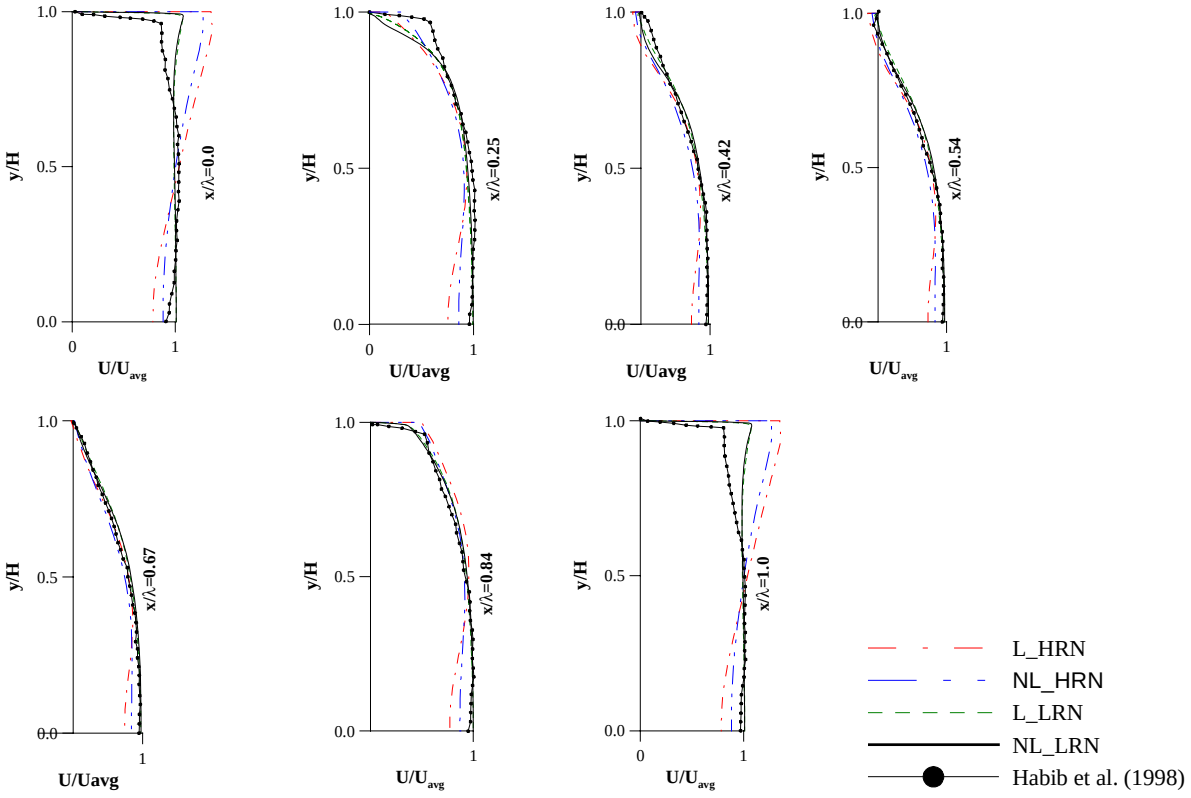

Figure 4 – Normalized axial velocity profiles.

5. CONCLUSIONS

In this work four models were investigated. The analysis was conducted to predict the turbulent flow field at Reynolds number of 40000 in a periodically symmetric converging-diverging channel. The low Reynolds number formulation utilized in the linear and non-linear k-ε models presented better agreement (for pressure drop) with the experimental data by Saniei and Dini (1993), as shown in Table 2. The smaller deviation was obtained by NL_LRN model.

An analysis of residue for the velocity component U along the solution relaxation process was done. It has been observed that for the present problem, the semi-implicit treatment of non-linear diffusive terms did not benefit the stability characteristics of the solution in relation to the fully explicit treatment when using either the High or the Low Reynolds formulation. Both treatments converged at the same rate. The semi-implicit treatment is relevant only when we make use of computational grids with control-volumes according to Fig. 1. Or say, for grids having the geometric distance $\Delta x_\eta^e = 0$ (see Figure 3), the semi-implicit treatment did not contribute to the robustness of the solution method.

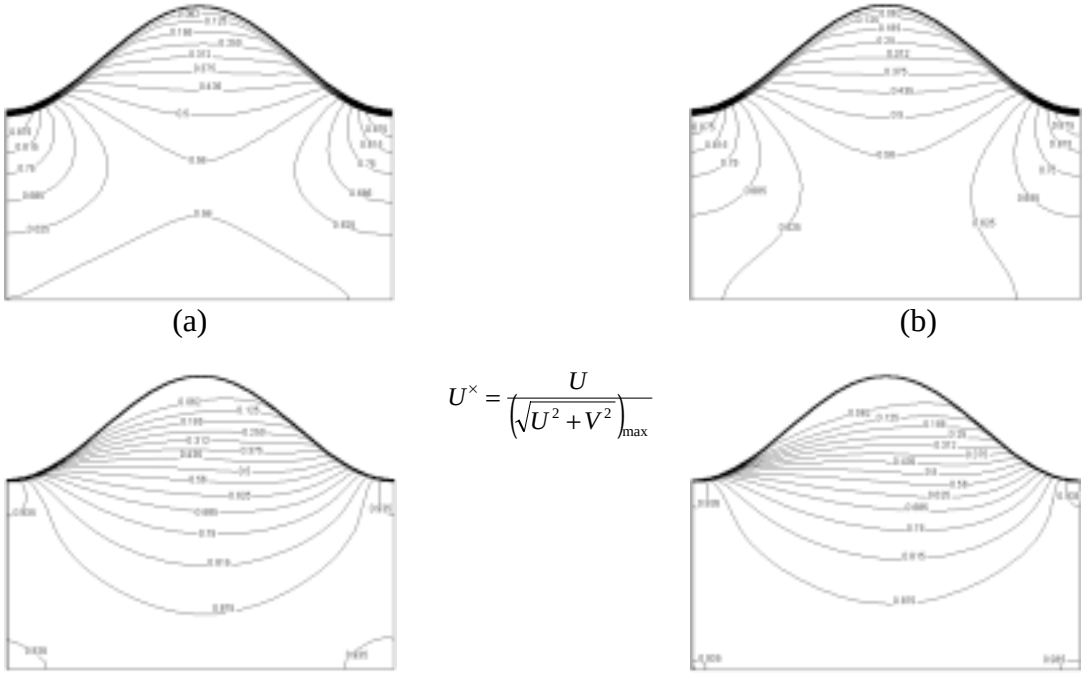

(a) (b)

$$U^{\times} = \frac{U}{\left(\sqrt{U^2 + V^2}\right)_{\max}}$$

(c) (d)

Figure 5 - Dimensionless velocity distribution, $U^{\times}$: (a) L_HRN; (b) NL_HRN; (c) L_LRN; (d) NL_LRN.

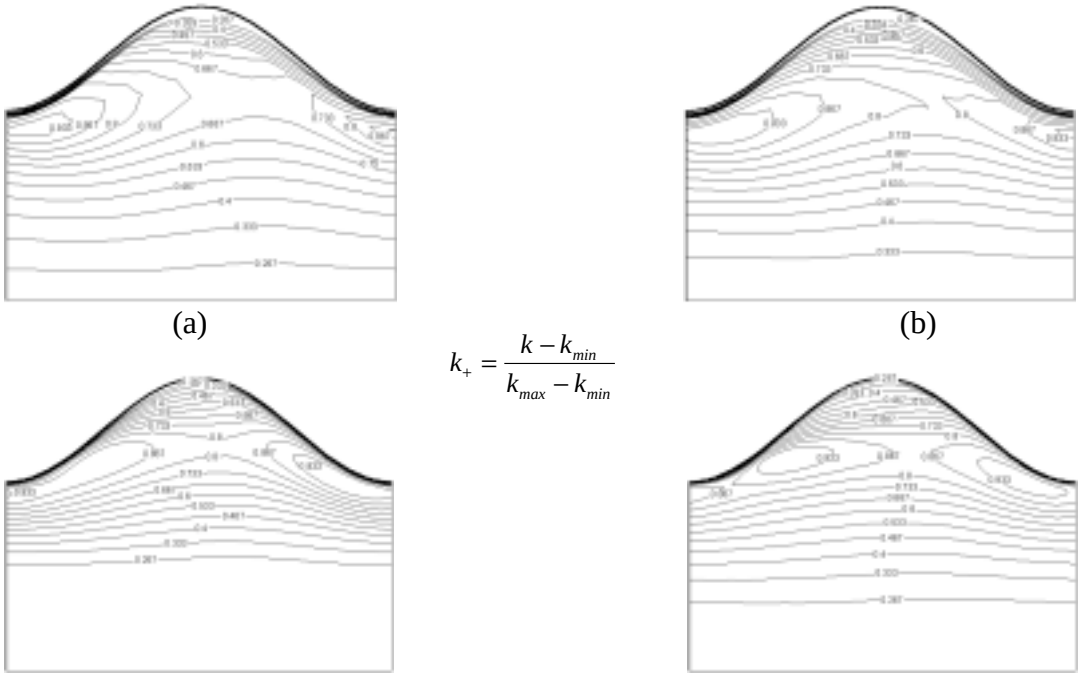

(a) (b)

$$k_{+} = \frac{k - k_{min}}{k_{max} - k_{min}}$$

(c) (d)

Figure 6 - Dimensionless k_{+} distribution: (a) L_HRN; (b) NL_HRN; (c) L_LRN; (d) NL_LRN.

6. ACKNOWLEDGEMENTS

The authors would like to thank FAPESP and CNPq, Brazil, for their financial support during the preparation of this work.

7. REFERENCES

Abe, K., Nagano, Y. and Kondoh, T., 1992, "An Improved k-ε Model for Prediction of Turbulent Flows with Separation and Reattachment", *Trans. JSME, Ser. B*, Vol.58, pp.3003-3010.

Assato, M. and de Lemos, M.J.S., 1998, "Development of a Non-Linear Turbulence Model for Recirculating Flows Using Generalized Coordinates", *ENCIT98- Proc. 7th Braz. Cong. Eng. Th. Sci.*, vol. 2, pp. 1386-1391, Rio de Janeiro, RJ, Nov. 3-6.

Assato, M. and de Lemos, M.J.S., 2001, "Numerical Simulation of Turbulent Flow Through Axisymmetric Stenosis Using Linear and Non-Linear Eddy-Viscosity Models", Proceedings of the 16th Brazilian Congress of Mechanical Engineering", Uberlândia/MG, Brazil.

Abid, R., Rumsey, C. and Gatski, T. B., 1995, "Prediction of Nonequilibrium Turbulent Flows with Explicit Algebraic Stress Models", AIAA J., 33 (11), pp. 2026-2031.

Bauer, W., Haag, O. and Hennecke, D.K., 2000, "Accuracy and Robustness of Nonlinear Eddy Viscosity Models", Int. J. Heat and Fluid Flow, Vol. 21, pp. 312-319.

Buckels, J., Hanratty, T.J. and Adrian, R.J., 1984, "Turbulent Flow over Large Amplitude Wavy Surfaces", Journal of Fluid Mechanics, 140, pp. 27-44.

Gatski, T.B. and Speziale. C.G., 1993, "On Explicit Algebraic Stress Models for Complex Turbulent Flows", J. Fluid Mech., Vol. 254, pp. 59-78.

Habib, M.A., Ikram Ul-Haq, Badr, H.M. and Said, S.A.M., 1998, "Calculation of Turbulent Flow and Heat Transfer in Periodically Converging-Diverging Channels", Computers & Fluids, Vol. 27, No. 1, pp. 95-120.

Hanratty, T.J., Abrams, J. and Frederic, K.A., 1983, "Flow over Solid Wavy Surfaces" In Structure of Complex Turbulent Shear Flow, IUTAM Symposium Marseille 1982, ed. R. Dumas, and L. Fulachier. Springer, Berlin, pp. 79-88.

Hsu, S.T. and Kennedy, J.F., 1971, "Turbulent Flow in Wavy Pipes", Journal of Fluid Mech., vol. 47, part 3, pp. 481-502.

Jones, W.P. and Launder, B.E., 1972, "The Prediction of Laminarization with Two-Equation Model of Turbulence ", Int. J. Heat & Mass Transfer, Vol. 15, pp. 301 - 314.

Launder, B.E. and Spalding, D.B., 1974, "The Numerical Computation of Turbulent Flows", *Comp. Meth. Appl. Mech. Eng.*, vol. 3, pp. 269-289.

Launder, B.E., Reece, G.J., Rodi, W., 1975, "Progress in the Development of a Reynolds Stress Turbulence Closure", J. Fluid Mech., 68, 537.

Nisizima, S. and Yoshizawa, A., 1987, "Turbulent Channel and Couette Flows Using an Anisotropic k-ε Model", AIAA J., Vol. 25, N^{0} 3, p. 414.

Patel, V.C., Chon, J.T. and Yoon, J.Y., 1991, "Turbulent Flow in a Channel with a Wavy Wall", Journal of Fluids Engineering, 113, pp. 579-586.

Pope, S.B., 1975, "A More General Effective-Viscosity Hypothesis", J. Fluid Mech., 72, pp.331.

Rahman, M., Rautaheimo, P. and Siikonen, T., 1997, "Numerical Study of Turbulent Heat Transfer from a Confined Impinging Jet using a Pseudo-Compressibility Method", In: Hanjalic, K., Peeters, T. (Eds.), Turbulence, Heat and Mass Transfer 2. Delf University Press, Delft, pp. 511-520.

Rubinstein, R. and Barton, J.M., 1990, "Renormalization Group Analysis of the Stress Transport Equation", Phys Fluids A2(8), pp. 1472-1476.

Saniei, N. and Dini, S., 1993, "Effects of height and geometry on local heat transfer and pressure drop in channel with corrugated walls", Heat Transfer Engineering, 14 (4), pp. 19-31.

Shih, T.H., Zhu, J. and Lumley, J.L., 1993, "A Realizable Reynolds Stress Algebraic Equation Model", NASA TM-105993.

Speziale, C.G., 1987, "On Nonlinear k-l and k- ε Models of Turbulence", J. Fluid Mech., vol. 176, pp. 459-475.

Zilker, D.P., Cook, G.W. and Hanratty, T.J., 1977, "Influence of the Amplitude of a Solid Wavy Wall on a Turbulent Flow, Non-Separated Flows", part 1. Journal of Fluids Mechanics, 82, pp. 29-51.